PAPER • OPEN ACCESS

Miniaturized thin-film filters to connect multiple self-written waveguides

To cite this article: A Günther *et al* 2023 *J. Opt.* **25** 065801

View the article online for updates and enhancements.

Miniaturized thin-film filters to connect multiple self-written waveguides

A Günther[1,2,5,*], K Kushwaha[2], A K Rüsseler[3,5], F Carstens[3], D Ristau[3,4,5], W Kowalsky[1,5] and B Roth[2,5]

[1] Institute of High Frequency Technology, Technical University Braunschweig, Schleinitzstraße 22, 38106 Braunschweig, Germany
[2] Hannover Centre for Optical Technologies, Leibniz University of Hannover, Nienburger Str. 17, 30167 Hannover, Germany
[3] Laser Zentrum Hannover e.V., Hollerithallee 8, 30419 Hannover, Germany
[4] Gottfried Wilhelm Leibniz Universität Hannover, Welfengarten 1, 30167 Hannover, Germany
[5] Cluster of Excellence PhoenixD (Photonics, Optics and Engineering—Innovation Across Disciplines), Welfengarten 1a, 30167 Hannover, Germany

E-mail: axel.guenther@ihf.tu-bs.de

CrossMark

Abstract

Self-written waveguides (SWWs) have been well investigated within the last decades. In most cases, they are used as low-loss coupling structures, i.e., to connect buried optical structures in photonic integrated circuits. In this work, we extend the field of possible applications for SWWs by embedding a novel thin-film filter to split the beam and connect multiple output ports simultaneously. The multilayer design of the dielectric filter can be customized to enable its application as a dichroic beamsplitter for photonic networks. The embedded thin-film filter was characterized in detail and used to connect an additional optical sensing element, which is also based on SWWs, to demonstrate its usability for measurement of physical quantities.

(Some figures may appear in colour only in the online journal)

1. Introduction

During the last decades, photonic structures have become increasingly important, as they can supersede their electronic counterparts, i.e., by reaching higher data transmission rates. Furthermore, they can be used for signal distribution in optical networks or as sensing elements, among others [1–6]. Polymer based components in particular have gained increased interest due to easier production processes and lower material costs [7]. Essential for this development is the investigation of efficient coupling structures to connect different types of waveguides, light sources and sensors, respectively. Common coupling structures such as mirrors, gratings or tapers in different shapes have been broadly investigated [8–11]. A new technique, which has evolved during the last decade, is the utilization of self-written waveguides (SWWs) as coupling elements [12–16]. These polymer based structures enable low-loss connections, i.e., between waveguides (regardless of their shape and size), fibers, light sources and detectors [17–19]. It was also shown that this approach allows for compensation of misalignment between the connecting components [17]. Such interconnects can be integrated into a broad field of fabrication processes, such as photolithography [20, 21], hot embossing [22] or direct laser ablation [23]. The unique properties of this interconnection also enables thermal sensing by monitoring the transmitted optical power [24, 25]. It is also possible to connect multiple components directly with each other, which was realized so far only using structures with a single splitter combining multiple laser beams [12, 26]. Another investigated

approach with regard to communication purposes was to build a polymer waveguide module for wavelength division multiplexing based on a thin-film filter [27, 28]. In general, there are various other techniques to realize beam splitting, for example, by using integrated optics as directional couplers [29–32], hybrid photonic-plasmonic polarization beam splitting [33] or grating structures [34], among others. These approaches can achieve very high coupling efficiencies, although a very high fabrication accuracy is required due to the small feature sizes in the nm-regime. They also mostly rely on relatively expensive materials.

In this work, we present a novel approach, in which a customized miniaturized thin-film filter element [35] was combined with an SWW to stably connect multiple outputs with one input port. Hereby, the flexibility and convenient processability of SWWs are especially advantageous with regard to the realization of optical networks for applications in short-distance sensing or monitoring where low intensity levels are usually sufficient. The higher optical attenuation of the polymer material used to manufacture the SWWs compared to their glass-based counterparts is in many such applications not a significant limitation. The chromatic separation by the thin-film filter enables additional functionalities, rendering these components interesting for beam combination or separation in several use cases. Here, we focus on the combination of an optical sensor with a reference beam split by a thin-film filter to enable measurement of the sensor signal and the source drift at the same time.

2. Fabrication process

The fabrication of SWWs is based on a photosensitive monomer. These interconnects are termed 'self-written' because the radiation itself, transmitted through the monomer, polymerizes the monomer locally, thus modifying the refractive index and creating the optical waveguide.

2.1. SWW

To create a self-written interconnect between a source and a detector in a photosensitive monomer, only a waveguiding component connected to a suitable light source or a light emitting element itself is required. The writing procedure is sketched in figure 1. As a first step, the two optical elements, i.e., waveguides, are aligned to each other for maximum optical transmission. Subsequently, the photosensitive monomer is applied on the interface of the two elements. Both waveguides are moved away from each other along their optical axis, allowing the fluid-like monomer to enter the gap between the two waveguides. Fine adjustment in X–Y direction can be performed by propagating light at a wavelength that is not absorbed by the monomer through one of the waveguides and re-alignment for maximum transmission. To write the SWW, light at a shorter wavelength, which is within the absorption profile of the monomer, is propagated through the waveguide. In our work, we use the commercially available UV-curable epoxy NOA68 from Norland Adhesive as
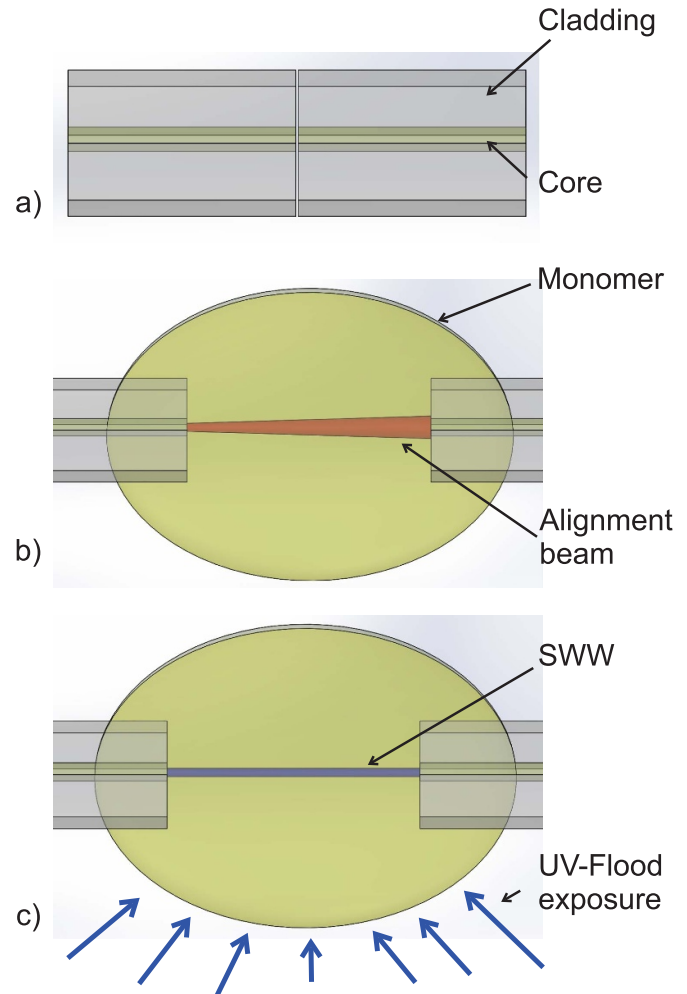

Figure 1. Scheme of the writing process of an SWW. (a) During the first step both components are aligned relative to each other. (b) Elements are moved away from each other along their optical axis and a drop of UV-curable monomer is applied. (c) Guiding UV-light through one of the waveguides starts the SWW writing process locally and leads to a straight self-written waveguide. Subsequently, the surrounding monomer is cured by flood exposure.

monomer with a writing wavelength of 406 nm. This can be generated by a suitable laser diode, but also higher wavelength sources are applicable, depending on the used photoinitiator in the monomer [17]. When the writing beam is propagated, the polymerization starts where the light enters the monomer, resulting in a local increase in the refractive index. Due to this process, the beam is guided inside the polymerized region and continues propagating straight until the written waveguide hits another surface or the beam intensity is less than the polymerization threshold. Finally, it is possible to cure the surrounding resin with UV flood exposure. In previous investigations, it was shown that the SWW still exists after the external curing. The refractive index difference between core (SWW) and cladding (substrate) is around 0.002 and enables efficient waveguiding [17]. The created SWW exhibits an attenuation value of $\alpha = 0.2\,\mathrm{dB\,cm}^{-1}$ at $\lambda = 638$ nm with the applied material (NOA68, Norland Adhesive)[25]. Using other monomers, which are sensitive to longer wavelengths,

even enabled the connection of different waveguides with an offset between their optical axes [17]. Even though the above attenuation values are higher compared to silica-based optical components such as waveguides and splitters, applications such as short-distance sensor arrays or process monitoring can benefit from the simplicity of the concept and the flexibility and cost-efficiency of the process.

2.2. Thin-film filter

In this work, we modify the standard writing process by integrating a thin-film filter element, which is placed on a 250 μm thick PMMA foil (thyssenkrupp Plastics GmbH, Germany) as substrate for better handling purposes (in this case) and splits the writing beam at $\lambda = 406$ nm with a polarization independent ratio of approximately 50:50 to a transmission and reflection path, respectively. This means that only 50% of the radiant flux in front of the filter element is available for writing each SWW branch after the beam splitting. Inside the dielectric filter and the substrate, waveguiding, as it occurs inside the polymerized monomer, is no longer effective and the beam diverges slightly. A miniaturized, substrate-free filter would reduce the crucial propagation length in the transmission direction and thus the beam divergence as well [35]. While a typical glass substrate has a thickness from one to a few millimeters, the substrate-free thin-film is much thinner, of the order of micrometers. By using such a filter without substrate, beam divergence inside the element and the risk that the transmitted radiant intensity during writing decreases below the polymerization threshold would be reduced much stronger. In this work, due to the writing of multi-mode waveguides where light coupling conditions are less crucial (compared to their single-mode counterparts), such beam distortion effects are less relevant. However, in the next steps of our work, the presented writing procedure will be used to create single mode waveguides where light coupling is more critical and, thus, filter elements without substrates will be used.

Another advantage of the substrate-free filters is that the thin-film design can be directly matched to the refractive index of the surrounding waveguide. To determine the dispersion of the NOA68 beyond the single wavelength value given in the data sheet, a refractive index profilometer (RINCK elektronik, Germany) was used. In this way, the refractive index of NOA68 as the surrounding medium was determined in the liquid state and after curing at 405 nm, 639 nm, 850 nm and 1308 nm obtaining values of 1.5097, 1.5091, 1.5013 and 1.4654, respectively, for the polymerized material.

A thin-film software [36] was used to create a multilayer design, which fulfills the filter specifications for the beam splitting wavelength region, the highly reflective wavelength region (HR) and the anti-reflective wavelength region (AR) as given in table 1. Specifications were demanded for all polarization states, because the polarization of the incoming light is unknown. It should be noted that since the filter is integrated at a large angle of incidence of 45°, it exhibits a (partly very large) polarization dependence at all wavelengths except those specified in table 1. The design was developed for the

Table 1. Specifications of the filter element for different wavelengths λ, angles of incidence (AoI), independent of the polarization state.

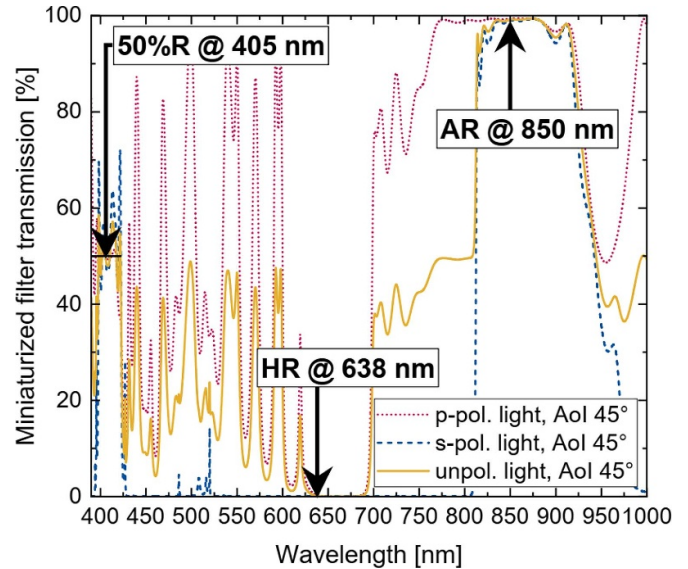| λ (nm)	AoI (°)	Specification	Functionality
406 ± 2	45 ± 1	$R = T = 50\% \pm 5\%$	Beam splitting
638 ± 2	45 ± 1	HR: $R > 98\%$	Demultiplexing
850 ± 2	45 ± 1	AR: $T > 98\%$	Demultiplexing

Figure 2. Modeled transmission of the miniaturized, substrate-free filter element when embedded into the SWW network. The data is shown for different polarization states of the incoming light (red dotted line for p-polarized light, blue dashed line for s-polarized light, yellow solid line for unpolarized light). The polarization independent specification wavelengths (cf table 1) are marked with black arrows.

two materials silica and titania, which exhibit a high refractive index contrast. The total thickness of the designed multilayer stack was 8.17 μm.

The filter design was deposited on sacrificial substrates in an ion beam sputtering process [35]. To achieve a high layer thickness accuracy, *in situ* process control with a high resolution optical broadband monitor was used [37]. With this monitoring system, the layer thicknesses are calculated from *in situ* transmission measurements on a fused silica sample. This monitoring sample is placed in the same substrate holder as the silicon wafers and is simultaneously coated in the same process run. From the changes in the broadband transmission spectrum of this sample, the produced multilayer stack is derived. Using thin-film software developed at Laser Zentrum Hannover e.V., a modeled transmission for the resulting spectral performance of the filter element when integrated into the SWW network was carried out. The modeled transmission results are shown in figure 2 for the case of an ideal alignment of the filter element to the SWW of 45°. The specifications according to table 1 are met, independent of the incoming light polarization state.

The finished coating was laser segmented into small elements with an edge length of 1 mm and the sacrificial substrate was removed, resulting in freestanding thin-film elements to be integrated into the SWW.

3. Measurement setup

The setup used in this work is sketched in figure 3. The experimental configuration consists of two three-axis high precision stages (MDE122, Mountain Photonics GmbH, Germany) with a fiber holder on top. Standard telecommunication fibers (OM2) with a core diameter of $50\,\mu$m were used for the connection with SWWs. These fibers are designed for longer wavelengths around $\lambda = 1300$ nm. However, attenuation measurements at the wavelengths relevant for this work ($\lambda = 638$ nm $- 940$ nm) resulted in less than $0.1\,\mathrm{dB\,m}^{-1}$. This is approximately 50 times less than the attenuation of the SWW and allows to neglect the effect of the fibers in our experiments [25]. The fiber end facets were placed on a 3D-printed mold, which contains grooves for the coarse adjustment of the fibers toward an additional slit for the filter. Three fiber end facets were aligned on this mold in the way that the angle of incidence on the thin-film filter is 45° and the angle between the fibers is 90°. The UV-curable monomer (NOA68, Norland Products Inc. USA) was applied on the mold and a fine adjustment was performed with the three-axis stages while maximizing the transmission signal of the alignment beam at $\lambda = 638$ nm. The filter itself had a size of $\approx$1 mm $\times$ 1 mm $\times$ 8 μm. For this experiment, the filter was placed vertically into the setup at an angle of $\approx$45° toward the incoming fiber. Additionally, the monomer needs to be applied around and at the position of the filter. Thus, it was helpful to stabilize the thin-film filter by fixation on a rectangular PMMA-sheet $\approx$10 mm $\times$ 30 mm $\times$ 250 μm to make sure that the filter stays in the right position and shape. Therefore, a drop of distilled water was used to avoid air inclusions in between the filter and the PMMA.

The writing process of the SWW was performed using the attached stabilized multi-channel diode laser module (MCLS1, Thorlabs Inc. USA), emitting coherent radiation at a wavelength of $\lambda = 406$ nm with an average power of $P_{406\,\mathrm{nm}} \approx$ 4.5 mW for writing the SWW and additionally at $\lambda = 638$ nm and $\lambda = 850$ nm with an average power of $P_{638\,\mathrm{nm}} \approx 15$ mW and $P_{850\,\mathrm{nm}} \approx 10$ mW, respectively, for characterization. Additional fiber coupled laser diodes (SPL785-50-PM-PD and SPL940-50-PM-PD, Roithner Laser Technik GmbH, Austria) at $\lambda = 785$ nm and $\lambda = 940$ nm with $P_{785\,\mathrm{nm}} \approx 50$ mW and $P_{940\,\mathrm{nm}} \approx 50$ mW were used for further characterization outside of the target wavelength range of the filter design. The optical transmission was monitored by means of fiber coupled photodiodes (S151C, Thorlabs GmbH, Germany) with the corresponding power meter (PM100USB, Thorlabs GmbH, Germany). The thin-film filter distributes the incoming beam into the two connected arms. For the characterization of the filter element, both arms were connected directly to the photo
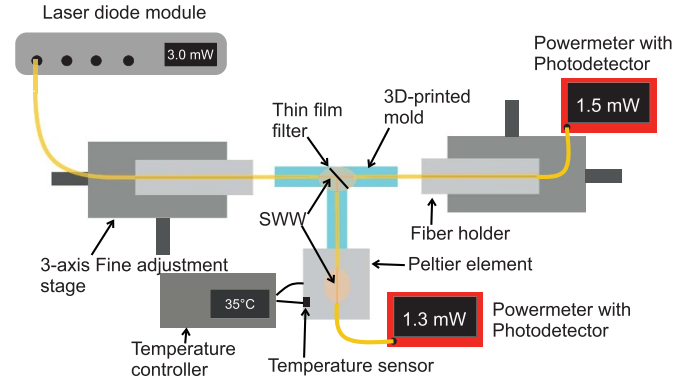

Figure 3. Sketch of the experimental setup for characterization of multiple SWWs connected by a thin-film filter. One of the connections is functionalized with a second SWW on a Peltier element. We vary the temperature of this arm while using the corresponding variation of the optical transmission of the SWW to measure the increase in temperature. The other arm is a reference to minimize environmental effects or fluctuations of the light source.
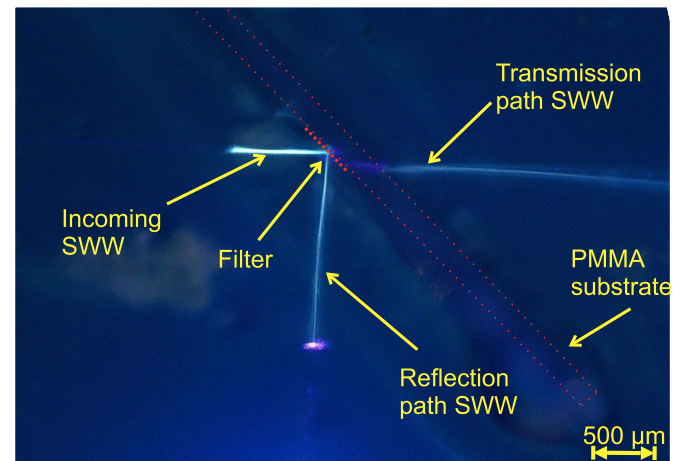

Figure 4. Microscope image of the thin-film filter, which is attached to a PMMA substrate and placed in between three fibers. The fluorescent light shows the writing process of the SWWs during the illumination with $\lambda_{\mathrm{writing}} = 406$ nm. The displacement of the incoming and transmitted SWW originates primarily from the refraction of the used PMMA-sheet. The elliptical shape of the resin surrounding the PMMA leads to aberrations so that the SWWs appear slightly bent in the image.

diodes. An image of the connected SWWs with the integrated thin-film filter element is shown in figure 4.

For further investigations, an additional SWW was created and connected to the reflected arm. This SWW is required to demonstrate the thermal sensing capabilities of the interconnect, similar to [25]. Therefore, it was placed on a Peltier element with a thermal sensor attached to control the temperature of the SWW precisely.

To fix all connections, the surrounding resin was finally cured by UV flood exposure using an UV LED with

a wavelength of $\lambda = 365\,\text{nm}$ and an average power of $P_{365\,\text{nm}} \approx 17\,\text{mW}$.

4. Results

After finishing the writing process of the SWWs, the performance of the thin-film filter embedded into the cured adhesive was thoroughly characterized. For this purpose, the optical transmission and reflection at various wavelengths were determined by attaching fiber coupled photodiodes to both output arms, without attaching the additional SWW for thermal sensing. The results of these measurements are summarized in table 2. The comparison of these measurements with the values obtained for the filter alone, see figure 2, shows that embedding of the thin-film filter does not affect its performance in terms of meeting the given specifications. In addition, all splitting ratios determined by the measurements coincide with the parameters of the designed element. The filter can also be designed for telecommunication wavelengths in the range of 1330 nm or 1550 nm, respectively. The SWWs have not been characterized for these wavelengths at this stage, however the datasheet of the pristine material suggests a sufficiently high transmittance in the NIR-range. Recent work has focused on the visible wavelength range so far.

Deviations of the measurements are only observed at the additional wavelengths of 785 nm and 940 nm, which are not included in the specifications for the filter design. The filter is specially designed to exhibit a $\pm 1°$ angle alignment tolerance at the specification wavelengths, see table 1. However, an imperfect adjustment of the filter towards the incoming fiber can still result in a great change of the transmission and reflection at other wavelengths for which no specifications are given. An angle misalignment of only $1.08°$ and a dominance of p-polarization in the incoming light (70% p-polarized) are sufficient to explain the measured splitting ratio at both 785 nm and 940 nm, see figure 5.

In a further step, a Peltier element (TEC1-127 060, TRU Components, Germany) with a thermal sensor (M222, Heraeus Nexensos GmbH, Germany) was attached to the reflected arm of the SWW. This is indicated in figure 3 as the waveguide being directed downwards. With this step, the applicability of the structure for temperature sensing was investigated. We have demonstrated that an increasing temperature yields an increasing optical transmission of the SWW originating from different thermo-optical coefficients of the core and cladding after the writing and curing process, respectively. This results in a different change of the refractive index with an increasing temperature, finally obtaining a larger numerical aperture of the SWW [24, 25].

To verify that changes in the transmission of this additional SWW path are from the applied change in temperature by the Peltier element, it is important to quantify how other environmental influences and laser fluctuations affect the measurement. The influence of these noise sources can be determined by integrating a reference arm into the measurement

Table 2. Measured optical power values in transmission and reflection of the connected SWWs using various input wavelengths. Hereby P_T gives the transmitted optical power and P_R the reflected one, respectively.

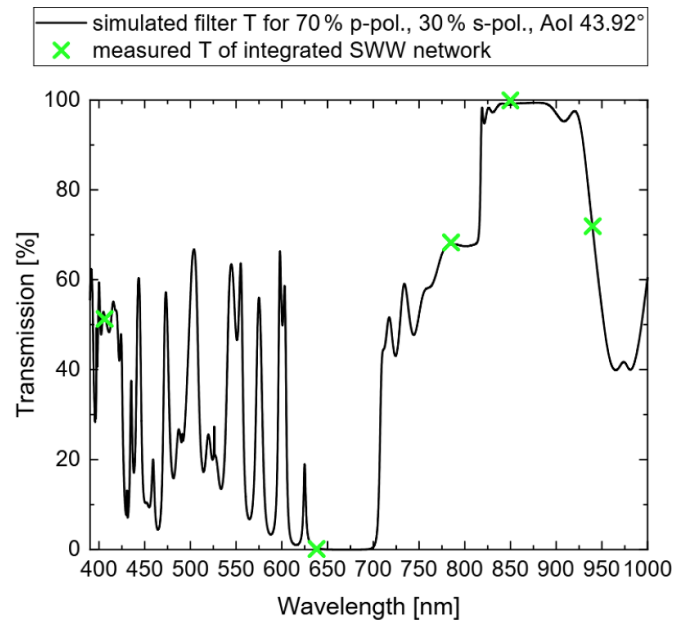| λ_{Input} (nm)	P_T (mW)	P_R (mW)	Splitting ratio (T:R)
406	0.98	0.93	51.3 : 48.7
638	$0.1 \cdot 10^{-3}$	4.20	0.1 : 99.9
785	7.18	3.34	68.3 : 31.7
850	9.00	$0.04 \cdot 10^{-3}$	99.9 : 0.1
940	15.10	5.90	71.9 : 28.1

Figure 5. Modeled transmission of the miniaturized, substrate-free filter element when embedded into the SWW network under an angle of incidence of $43.92°$, for the case where the incoming light is 70% p-polarized and 30% s-polarized (black line). The green crosses indicate the measured transmission ratios of the SWW network, cf table 2.

setup, which was realized with the transmission path, directed to the right in figure 3. This feature enables monitoring of the system's performance during the temperature measurement. The results of such an experiment are shown in figure 6. The comparison of the two graphs in figure 6 shows that the increase in the optical transmission through the arm containing an additional SWW for temperature measurement only comes from the heating by the Peltier element. The monitoring of the optical transmission through the reference arm showed a nearly constant behavior and seems unaffected by the temperature change. The highest sensitivity for thermal sensing was achieved at a wavelength of 638 nm, with a change of the optical intensity of $0.8\%\,\text{K}^{-1}$. The higher noise level of the reference arm is due to the filter's splitting ratio at this wavelength. It was designed to be highly reflective at 638 nm, therefore the transmission is relatively low, which led to measured power values in the reference arm in the range
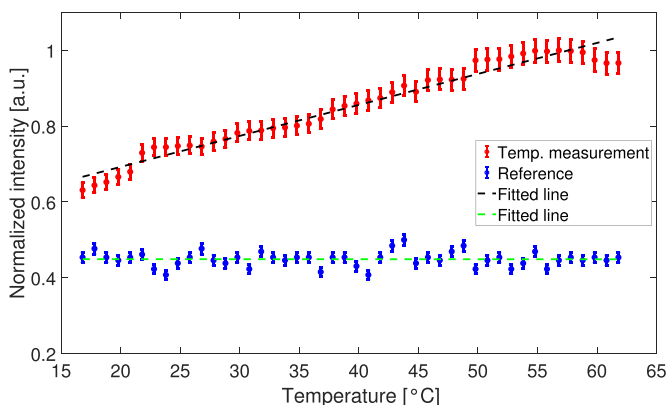
Figure 6. Regression lines and the corresponding error bars of the temperature measurement using the SWW placed on the Peltier element (red) with a connected reference arm attached directly to a photo diode using the thin-film filter (blue) with the corresponding fitted lines. The error is mainly based on the inaccuracy of the power meter given with ±3%. The normalized intensity of the reference arm was divided by two for better visibility.

of ≈50 nW, which is well within the measurement range of 1 nW–20 mW.

5. Conclusion

In this work, we have integrated a thin-film filter element into an optical interconnect consisting of SWWs, which enables a splitting of the writing beam to create an optical network-like structure containing multiple SWWs simultaneously. We have shown that embedding of the filter does not impair its performance. This opens a wide field of further applications, in particular, when connecting multiple ports and addressing them with lasers at different wavelengths. Utilization as an additional feature for optical sensors, which are based on waveguides offering a reference beam path, is also possible and demonstrated in this work as well. Future work will focus on the integration of customized filters to optimize the sensing performance, i.e., to achieve a higher sensitivity for thermal sensing. Various other sensor concepts will also be investigated, i.e., for measuring humidity or a novel highly sensitive distance sensor. Finally, more complex and extended planar networks will be realized to investigate their suitability for distributed sensing.

Data availability statement

All data that support the findings of this study are included within the article (and any supplementary files).

ORCID iDs

A Günther ⓘ https://orcid.org/0000-0003-4244-4438
A K Rüsseler ⓘ https://orcid.org/0000-0003-1215-283X
F Carstens ⓘ https://orcid.org/0000-0002-4841-358X
B Roth ⓘ https://orcid.org/0000-0001-9389-7125

References

[1] Guimard N K, Gomez N and Schmidt C E 2007 *Prog. Polym. Sci.* **32** 876–921
[2] Keil N, Zhang Z, Zawadzki C, Wagner C, Scheibe A, Ehlers H, Ristau D, Wang J, Brinker W and Grote N 2009 *Electron. Lett.* **45** 1167–68
[3] Zheng Y, Bremer K and Roth B 2018 *Sensors* **18** 1436
[4] Bremer K, Reinsch T, Leen G, Roth B, Lochmann S and Lewis E 2017 *Sens. Actuator* A **256** 84–88
[5] Rezem M, Günther A, Roth B, Reithmeier E and Rahlves M 2017 *J. Light. Technol.* **35** 299–308
[6] Terasawa H and Sugihara O 2021 *J. Light. Technol.* **39** 7472–78
[7] Dangel R, Hofrichter J, Horst F, Jubin D, La Porta A, Meier N, Soganci I M, Weiss J and Offrein B J 2015 *Opt. Express* **23** 4736–50
[8] Wang F, Liu F and Adibi A 2009 *Opt. Express* **17** 10514–21
[9] Wang L, Li Y, Porcel M G, Vermeulen D, Han X, Wang J, Jian X, Baets R, Zhao M and Morthier G 2012 *J. Appl. Phys.* **111** 114507
[10] Morimoto Y and Ishigure T 2016 *Opt. Express* **24** 3550–61
[11] Shani Y, Henry C H, Kistler R C, Orlowsky K J and Ackermann D A 1989 *Appl. Phys. Lett.* **55** 2389–91
[12] Xin F, Flammini M, Di Mei F, Ludovica F, Pierangeli D, Agranat A J and DelRe E 2019 *Phys. Rev. Appl.* **11** 1830–33
[13] Shoji S, Kawata S, Sukhorukov A A and Kivshar Y S 2002 *Opt. Lett.* **27** 185–7
[14] Malallah R, Cassidy D, Muniraj I, Ryle J P, Healy J J and Sheridan J T 2018 *Appl. Opt.* **57** E80–E88
[15] Malallah R, Li H, Muniraj I, Cassidy D, Al-Attar N, Healy J J and Sheridan J T 2018 *J. Opt. Soc. Am.* B **35** 2046–56
[16] Mohammed P A, Mahmood S Q, Aziz S B and Mohammed B K 2022 *Opt. Fiber Technol.* **68** 102792
[17] Günther A, Schneider S, Rezem M, Wang Y, Gleissner U, Hanemann T, Overmeyer L, Reithmeier E, Rahlves M and Roth B 2017 *J. Light. Technol.* **35** 2678–84
[18] Missinne J, Beri S, Dash M, Bosman E, Dubruel P, Watte J and Van Steenberge G 2013 *Adv. Photonics* (https://doi.org/10.1364/IPRSN.2013.JT3A.7)
[19] Violakis G, Bogris A, Pispas S, Fytas G, Loppinet B and Pissadakis S 2021 *Opt. Lett.* **46** 5437–40
[20] Nguyen H H D, Hollenbach U, Ostrzinski U, Pfeiffer K, Hengsbach S and Mohr J 2016 *Appl. Opt.* **55** 1906–12
[21] Tung K K, Wong W H and Pun E Y B 2005 *Appl. Phys.* **80** 621–6
[22] Rezem M, Günther A, Rahlves M, Roth B and Reithmeier E 2016 *Proc. Technol.* **26** 517–23
[23] Zakariyah S S, Conway P P, Hutt D A, Selviah D R, Wang K, Rygate J, Calver J and Kandulski W 2011 *J. Light. Technol.* **29** 3566–76
[24] Günther A, Baran M, Kowalsky W and Roth B 2021 *Appl. Sci.* **17** 7881
[25] Günther A, Baran M, Garg R, Roth B and Kowalsky W 2021 *Opt. Lasers Eng.* **151** 106922
[26] Malallah R, Cassidy D, Wan M, Muniraj I, Healy J J and Sheridan J T 2020 *Polymers* **12** 1438
[27] Yonemura M, Kawasaki A, Kato S, Kagami M and Inui Y 2005 *Opt. Lett.* **30** 2206–8

[28] Yamashita T, Kawasaki A, Kagami M, Yasuda T and Goto H 2010 *IEEE CPMT Symp. Japan* 1–4

[29] Alrifai R, Coad V, Alhaddad T, Taleb H, Rangelov A A and Montemezzani G 2023 *Phys. Rev.* A **107** 013527

[30] Love J D and Riesen N 2012 *Opt. Lett.* **37** 3990–2

[31] Song K Y, Hwang I K, Yun S H and Kim B Y 2002 *IEEE Photonics Technol. Lett.* **14** 501–3

[32] Leuthold J 2001 *J. Light. Technol.* **19** 700–7

[33] Ahmadivand A 2014 *Opt. Laser Technol.* **58** 145–50

[34] Dong Y, Yang J, Xu Y, Zhang B and Ni Y 2021 *IEEE Photon. J.* **13** 6600312

[35] Rüsseler A K, Gehrke P, Carstens F, Hoffmann G-A, Schönsee G, Thiel A, Vitt M Wienke A and Ristau D 2023 *Appl. Opt.* **62** B188–94

[36] Dieckmann M 2022 SPEKTRUM 32 design software (available at: www.lzh.de)

[37] Carstens F, Ehlers H, Schlichting S, Jensen L and Ristau D 2019 *OIC, OSA Tech. Digest* WA-7